New Journal of Physics
The open access journal at the forefront of physics

Deutsche Physikalische Gesellschaft DPG
IOP Institute of Physics

Published in partnership with: Deutsche Physikalische Gesellschaft and the Institute of Physics

OPEN ACCESS

RECEIVED
12 September 2019

REVISED
6 December 2019

ACCEPTED FOR PUBLICATION
11 December 2019

PUBLISHED
22 January 2020

Original content from this work may be used under the terms of the Creative Commons Attribution 3.0 licence.

Any further distribution of this work must maintain attribution to the author(s) and the title of the work, journal citation and DOI.

PAPER

THz generation from laser-induced breakdown in pressurized molecular gases: on the way to terahertz remote sensing of the atmospheres of Mars and Venus

Peter M Solyankin[1,2], Irina A Nikolaeva[3], Andrey A Angeluts[3], Daniil E Shipilo[3,4], Nikita V Minaev[5], Nikolay A Panov[3,4], Alexei V Balakin[1,2,3], Yiming Zhu[1], Olga G Kosareva[3,4,7] and Alexander P Shkurinov[1,2,3,6]

[1] Terahertz Technology Innovation Research Institute, Shanghai Key Laboratory of Modern Optical System, Terahertz Spectrum and Imaging Technology Cooperative Innovation Center, University of Shanghai for Science and Technology, Shanghai 200093, People's Republic of China
[2] ILIT RAS—Branch of the FSRC 'Crystallography and Photonics' RAS, Svyatoozerskaya 1, 140700, Shatura, Moscow Region, Russia
[3] Faculty of Physics and International Laser Center, Lomonosov Moscow State University, Leninskie Gory, Moscow 119991, Russia
[4] Lebedev Physical Institute of Russian Academy of Sciences, 53 Leninskiy prospect, Moscow 119991, Russia
[5] Federal Scientific Research Centre 'Crystallography and Photonics' of Russian Academy of Sciences, Moscow, Russia
[6] The National University of Science and Technology MISiS, Moscow 119049, Russia
[7] Author to whom any correspondence should be addressed.

E-mail: a.v.balakin@physics.msu.ru, ymzhu@usst.edu.cn and kosareva@physics.msu.ru

Keywords: terahertz generation, two-color optical breakdown, femtosecond pulse propagation

Abstract

The present paper studies the generation of terahertz (THz) radiation in CO_2 in comparison with atmospheric air at a wide range of pressures. We established experimentally and explained theoretically that for these gases there are optimal pressures at about 1 bar for air and 0.5 bar for CO_2 under which the efficiency of conversion from near-infrared to THz frequencies is the highest. We consider the possibility of applying femtosecond laser-induced THz generation for the study of the atmosphere of Mars and found that the overall THz yield near the surface of Mars is just a factor of 6 lower than on Earth. Comparable THz energy on the two planets is associated with underdense plasma on Earth (~10% of neutrals) and full double ionization of carbon dioxide on Mars (~200% of neutrals), the latter opening great perspective for THz remote sensing of trace gases in the Martian atmosphere.

1. Introduction

The generation of electromagnetic radiation that is produced by electromagnetic wave packets rapidly moving in a medium and acting on the electrons was first suggested by Askar'yan back in 1962 [1]. Even earlier Cherenkov described the generation of transition electromagnetic radiation by passage of fast particles [2]. Later, with the invention of lasers, which generate ultra-short light pulses, their ideas led to the formation of a novel field of research—terahertz (THz) photonics of isotropic medium. The works [3] and later [4] initiated the development of THz air photonics [5]. Very recently a rising interest of scientists to conversion of optical to THz radiation in liquids has appeared [6, 7]. Nowadays, the ideas of our predecessors have been implemented on a new level and enabled scientists to obtain extremely high THz fields [8]. With today's level of knowledge in the field of plasma physics and nonlinear optics we can very well understand that the phenomena, which lead to generation of electromagnetic radiation in gases and liquids under the action of ultra-short pulses, are an interesting example of dialectical unity of opposites. On the one hand, a considerable role is played by an ionized electron moving under the action of laser radiation [2, 9]. On the other hand, the nonlinearity of neutrals also plays an important role [10]. Besides, the resonant nonlinearity related to the excitation of electronic, vibrational and rotational states in atoms and molecules of the media can contribute to THz yield [11].

We can expect that by changing a gas pressure we can alter partial contributions of free electrons and the nonlinearity of neutrals to the overall nonlinear response of gaseous media under the action of high-intensity

© 2020 The Author(s). Published by IOP Publishing Ltd on behalf of the Institute of Physics and Deutsche Physikalische Gesellschaft

light field. One of the most important factors affecting the nonlinear response of the medium is the change of the conditions for laser-induced plasma production with pressure variation. For DC-biased single-color filament in dry nitrogen at pressures of 1–46 bar, the THz peak-to-peak yield was found to be independent of the gas pressure and comparable with the yield from GaAs THz sources [12]. In contrast, in the case of dual-color filament, the growth of air pressure results in two-order of magnitude increase in THz field at low pressures (3–100 mbar) and then one-order of magnitude decrease at high pressures (2–20 bar) [13]. The maximal THz field was detected at atmospheric pressure. The linear increase of THz field for the pressures 3–100 mbar was explained by the effect of almost full ionization of air molecules in the focus. The dual-color scheme with 800 + 400 nm, 40 fs, 6 mJ pulses allowed the authors of [14] to receive a microjoule level THz yield from Ar, Kr and Xe at the maximum pressure studied of 0.93 bar. Important observation was that for the gas pressure range between 0.1 and 0.93 bar the THz yield saturates and even decreases with the pressure increase. This was attributed to the phase slippage in the plasma. However, only one-dimensional numerical simulations were performed to dig into the reasons of this saturation. For the similar to [14] experimental setup, the saturation of THz yield with pressure increase up to 1 bar and fine control of THz radiation ellipticity by means of pressure variation were demonstrated in [15]. The change of THz field polarization from linear to circular is the evidence for the nonlinear interaction increase with the pressure. Diligent study of THz yield in a long 1.75 m cell for different gases and pressures of 0.1–0.9 bar confirmed that THz yield decreases with pressure in both air and carbon dioxide [16]. The authors of [16] also show that not only the tight focus but also comparatively long filament plasma channel leads to high optical radiation to THz conversion efficiency. These THz yield studies in the cell are important preliminary experiments for further advancement of THz technologies to atmospheric remote sensing applications [17]. However, remote THz generation in the Earth's atmosphere is limited owing to the challenge of dealing with high ambient moisture absorption as well as dispersion of the air components.

The purpose of the present paper is the study of the properties of pulsed THz radiation from two gases: CO_2 and air under different pressures. The choice of CO_2 is not accidental: this gas is prevalent (more than 95%) in the atmosphere of two planets—Mars and Venus, which are the focus of numerous space research programs. By the way, the ground Martian atmosphere corresponds to the small gas pressure of 6 mbar [18], whereas the atmosphere of Venus is the case of extremely high pressure of 93 bar [19]. The important feature of the Martian atmosphere is the absence of water vapor (~0.03% [20]), which is the main absorbing agent of THz radiation.

In the present work we study both low and high pressure ranges (0.01–1.5 bar with a step of 50–100 mbar and 2–10 bar with a step of ~1 bar) and aim to define the optimum pressure to receive the maximum THz yield from a two-color filament formed in strongly dispersive molecular gases in the conditions close to the ones near the surface of Earth or Mars. For the generation of THz radiation we used a scheme of mixing the independently controlled pulses of the fundamental 800 nm laser beam at a frequency ω with its second harmonic 2ω. In the simulations we used UPPE [21] to calculate the THz yield from a femtosecond filament at different pressures in air or carbon dioxide with absorption and refraction of gas mixtures included. The largest optical to THz conversion efficiency in the experiment in agreement with the simulations is obtained at about 1 bar in air and 0.5 bar in CO_2. The combination of a wide range pressure scan and 3D+time carrier resolved simulations is the novel approach yielding the clear picture of THz radiation from a cell with gas under variable pressures. The overall THz yield near the surface of Mars is just a factor of 6 lower than on Earth. Comparable THz energy on the two planets is associated with underdense plasma on Earth (8.7% of neutrals) and full double ionization of carbon dioxide on Mars (200% of neutrals), the latter opening great perspective for THz remote sensing of trace gases in the Martian atmosphere.

2. Experimental

In our experiments we studied the process of THz generation in laser-induced breakdown in air and CO_2 within a wide pressure range from 0.01 to 250 bar. We used two types of gas cuvettes—for high and low pressure. In these cuvettes we controlled the gas pressure to simulate the conditions of the Martian and Venus atmospheres, with CO_2 dominating in the THz generation process. The first cuvette should maintain a pressure of 0.01–3 bar and have a large-aperture Teflon outlet window, while the second one should operate in the range of 1–250 bar, allowing to reach gaseous, liquid and supercritical fluid state of CO_2. The entrance and exit windows of the cuvette were made of 10 mm thick sapphire and had an aperture diameter of 8 mm. The cuvettes, which were fabricated specially for our experiments, are described in details in our earlier publication [22]. Carbon dioxide with a purity of 99.9% and atmospheric air with humidity less than 10% were used as media for THz generation.

The experimental setup with independent control of ω and 2ω beams is shown in figure 1, see [23] for the details. The Ti:Sapphire laser radiation was divided into two parts by the beam splitter (BS). One of the beams was doubled in frequency with a 0.3 mm thick BBO type I crystal. Due to the dispersion in the input window and gaseous media in the cuvette, the group walkoff between the pulses of the first and second harmonics were

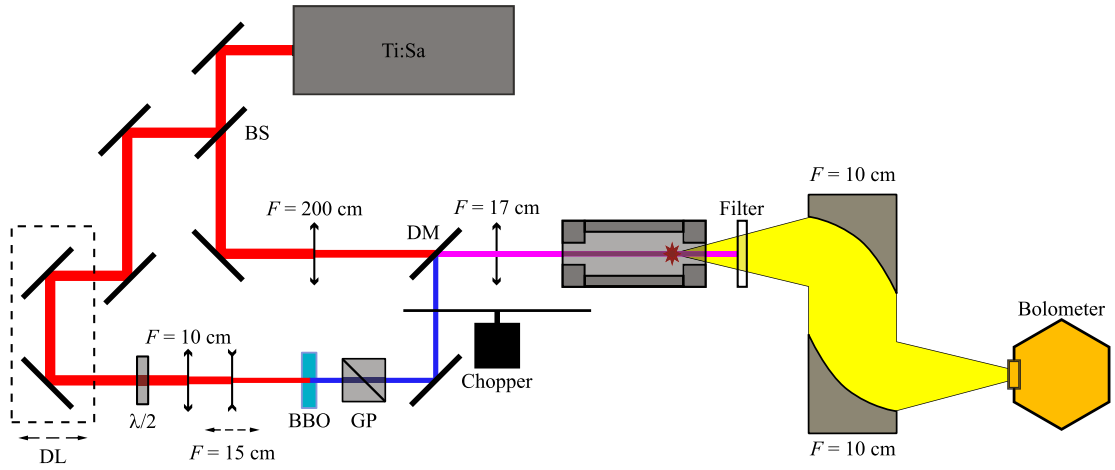

Figure 1. Experimental setup for THz generation in gases under varied pressure. BS: beamsplitter, DM: dichroic mirror, DL: delay line, filter: teflon and silicon plates, GP: Glan prism.

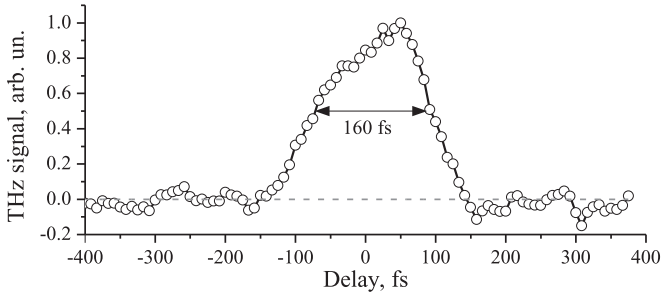

Figure 2. The dependence of THz generation efficiency on the delay between the first and the second harmonic pulses varied with the delay line at $p = 8.2$ bar CO_2 pressure. The routine procedure of group delay optimization was performed for every pressure independently.

adjusted for every pressure studied using the delay line DL to create two-color filament. A typical dependence of THz yield on the temporal delay is shown in figure 2.

The spatial adjustment of the first and the second harmonic beam sizes was performed with 200 cm focal length lens and a telescope. Then the beams were combined using a dichroic mirror DM and focused into the medium under study with a 17 cm focal length ultraviolet quartz lens. The vacuum beam diameters of ω and 2ω fields are estimated as 25 and 12 μm. The overlap of laser beams in the transverse direction was provided by the tilt of the pair of mirrors. Final adjustment of the overlap of the ω and 2ω beams geometrical focus positions along the optical axis is controlled by displacement of the telescope lenses located in the doubled frequency channel in front of the nonlinear crystal. This routine was done for the pressure of 1 bar. For other pressures we checked that the optimal spatial overlap between the harmonics was preserved.

THz radiation was collected by an off-axis parabolic mirror with a focal length of 10 cm, and was either focused on a bolometric detector by other parabolic mirror or directed to an interferometer (not shown in figure 1, see the details in [10]) to determine the spectral composition of the radiation. By means of the bolometer placed after the Michelson interferometer we registered the autocorrelation function of THz radiation, which was Fourier transformed to obtain spectrum. To facilitate the operation of the lock-in amplifier, the beam in the second harmonic channel was modulated by a chopper. The energy of the fundamental and the second harmonic pulses was 600 μJ and 40 μJ, respectively.

THz spectra of the radiation generated in the plasma of an optical breakdown of gases are shown in figure 3. The strong decline of the spectrum on the high-frequency side could be attributed to the decrease of transmission in the sapphire output window of the cuvette, which becomes significant above 1.5 THz, see the absorption spectrum of our sapphire window in figure 3 (dashed blue curve, right axis). It was reconstructed from the two THz spectra measured at the output of cell with 1 bar of air inside. The sapphire window was either installed or removed.

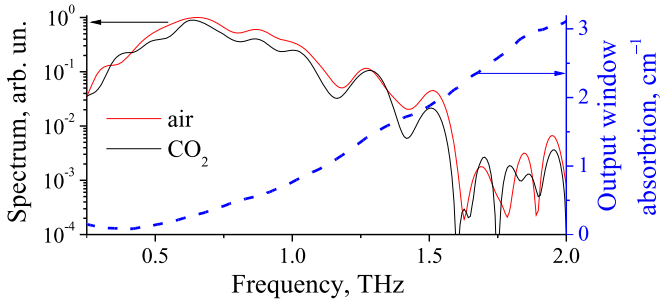

Figure 3. Spectra of THz signal generated in CO_2 (red curve) and in air (black curve). Blue curve corresponds to the right axis and represents the cuvette window absorption spectrum.

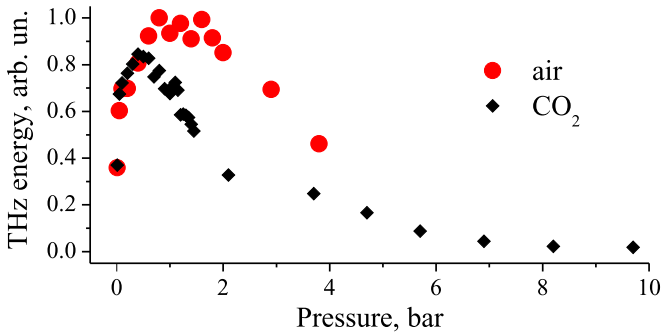

Figure 4. Dependence of THz yield on gas pressure in CO_2 (black rhombus) and air (red circles).

Figure 4 shows the dependence of the integrated THz signal measured by the bolometer on the gas pressure in the cuvette. In a high-pressure cuvette filled with CO_2, the pressure range up to 120 bar was investigated. For the pressures above 15 bar and under the room temperature, THz signal has no longer been detected. Therefore, with a pressure increase from 1 to 15 bars the THz yield slowly decreased from its maximum to the noise level of 0.01 as compared with the maximum value (figure 4, the higher pressure branch of the curve marked by black rhombus). In contrast, for a factor of 100 pressure decrease, the THz yield decreases just by a factor of 2 (figure 4, the lower pressure branch of the curve marked by black rhombus).

3. Simulations of the divergent electromagnetic radiation in variable density gases

The main variable parameter in our simulations is the pressure of the gas. Throughout the paper we will use the pressure p in bars as dimensionless coefficient. We restrict ourselves to the pressure of 10 bar. This is well below the critical pressure for CO_2 (73 bar), N_2 (34 bar), and O_2 (50 bar). Thus, we can assume gases as the ideal ones and scale the material parameters linearly with pressure in the following. For ~100 fs pulse and pressure below 10 bar we can also neglect the avalanche ionization.

Unidirectional pulse propagation equation (UPPE) [21] is widely used for investigations of THz emission from filaments [10, 24, 25]. It describes the nonlinear evolution of optical and terahertz fields self-consistently, including defocusing of the pump fields in the plasma, cross-focusing of the second harmonics and THz, other spatio-temporal effects. The linearly polarized light field $E(\tau, r, z)$ is assumed to be axially symmetric with $r(z)$ being the transverse (longitudinal) coordinate and τ being the time in moving reference frame. The spatio-temporal harmonic $\hat{E}(\omega, k_r, z)$ of the field $E(\tau, r, z)$ propagates in the forward direction and is governed by

$$\left(\frac{\partial}{\partial z} - \mathrm{i}k_z\right)\hat{E}(\omega, k_r, z) = \frac{2\pi\omega}{c^2 k_z}(\mathrm{i}\omega\hat{P}(\omega, k_r, z) - \hat{J}(\omega, k_r, z)), \quad (1)$$

where $k_z = \sqrt{\omega^2 n^2(\omega)/c^2 - k_r^2}$ is the longitudinal projection of the wave-vector, $n(\omega)$ is the refractive index, and c is the speed of light.

We assume that the pulse propagates from the lens to the cuvette entrance window in air with frequency-dependent refractive index $n_{\mathrm{air}}(\omega)$. Inside the cuvette, material dispersion obeys [26, 27]

$$n(p, \omega) - 1 = p(n_{\mathrm{bar}}(\omega) - 1). \tag{2}$$

Here $n_{\mathrm{bar}}(\omega)$ is the refractive index of the cuvette gas at atmospheric pressure. For air, we use Cauchy equation [28], for CO_2, we use HITRAN [29] data for resonant part and the fit from [30] for the optical range.

The polarization

$$P(\tau) = p\chi^{(3)}_{\mathrm{bar}}E^3(\tau) \tag{3}$$

represents the 3rd-order nonlinear response of bound electrons [31], where $\chi^{(3)}_{\mathrm{bar}}$ is the nonlinear susceptibility of the cuvette gas at 1 bar pressure. It lacks frequency dispersion, so we do not reproduce the possible resonant nonlinear response of CO_2, i.e. the delayed nonlinear response due to significant excitation of rovibrational transitions. This delayed response can, in principle, alter the generation and propagation of THz field. However, its inclusion requires the solution of quantum-mechanical equations for multi-level system in each spatial node. In that case, one has to solve thousands of ordinary differential equations for each point in space instead of just a few in our case, so the time required for simulations would grow up accordingly from total of several months to many years. The $(t, r + z)$ propagation simulations with inclusion of nonlinear rovibrational response are possible only if one truncates this system to the system consisting fewer ordinary differential equations [32]. However, the validity of this truncation [32] is limited to the intensity of ~10 TW cm^{-2}. In our experiment and simulations the intensity up to ~1000 TW cm^{-2} is attained, therefore the truncation suggested in [32] cannot be applied straightforwardly in our experimental conditions.

Indeed, the calculation of vacuum intensity in the geometry of our experiment yields $I_v \approx 2$ PW cm^{-2}. It is enough for full double and ~50% triple ionization of molecules considered. So we calculate the density of j-times ionized molecules N_j according to the rate equations [26]

$$\begin{aligned}
\frac{\partial N_0}{\partial \tau} &= -w_1(E)N_0,\\
\frac{\partial N_1}{\partial \tau} &= w_1(E)N_0 - w_2(E)N_1,\\
\frac{\partial N_2}{\partial \tau} &= w_2(E)N_1 - w_3(E)N_2,\\
\frac{\partial N_3}{\partial \tau} &= w_3(E)N_2
\end{aligned} \tag{4}$$

with the initial conditions $N_j(\tau \to -\infty) = pN_{00}\delta^0_j$, where $N_{00} = 2.7 \times 10^{19}$ cm^{-3} is the neutral density under the atmospheric pressure, and δ^l_j is the Kronecker delta; w_j are tunnel ionization rates for the jth-order ionization. The free electron density is therefore $N_e = N_1 + 2N_2 + 3N_3$. The material current J is represented by the sum of the free electron photocurrent J_e [9] and the absorption current J_a:

$$\frac{\partial J_e}{\partial \tau} = \frac{e^2}{m_e}N_e(\tau)E(\tau) - p\nu_c J_e(\tau); \tag{5}$$

$$J_a(\tau) = \frac{1}{E(\tau)}\frac{\partial}{\partial \tau}[U_1 N_1(\tau) + U_2 N_2(\tau) + U_3 N_3(\tau)]. \tag{6}$$

Here e and m_e are electron charge and mass, $\nu_c \approx 5$ ps^{-1} is the collision rate, U_j is the jth order ionization potential of a specie (N_2, O_2, or CO_2).

In order to decrease the computational time, we avoided the simulations of the first propagation stage governed solely by geometrical focusing similarly to our previous work [33]. We translate the initial conditions for the UPPE (1) from $z = 0$ to the cuvette entrance $z = z_0 = 12$ cm and apply the linear solution for the propagation of the broadband pulse up to z_0 in air under atmospheric pressure. From z_0, the nonlinear solver was used with the gas and pressure under consideration.

We assume the input field to be linearly polarized:

$$E(\tau, r, z = 0) = \mathrm{e}^{-r^2/2a_0^2} \times (E_1\mathrm{e}^{-\tau^2/2\tau_1^2}\cos(\omega_0\tau) + E_2\mathrm{e}^{-(\tau+\tau_{\mathrm{gd}})^2/2\tau_2^2}\cos(2\omega_0\tau + \varphi)), \tag{7}$$

where E_1 and E_2 are the electric field amplitudes corresponding to energies of 1.4 mJ and 10 μJ, $2\tau_1 = 125$ fs and $2\tau_2 = 85$ fs are durations of the 1st and 2nd harmonics, respectively; τ_{gd} is group delay compensation between them; φ is a relative phase; the input beam diameter is $2a_0 = 3$ mm. Geometrical focusing is described by multiplying (7) by the phase factor $\exp[\mathrm{i}\omega r^2/(2cF)]$ in the frequency domain, where $F = 15$ cm is the focal length.

In the experiment the group delay τ_{gd} between harmonics is optimized (figure 2) independently for each pressure, and random fluctuations of a phase between harmonics φ appear in each laser shot. For every given pressure, we perform three runs of UPPE solver so as to account for these experimental features. In the first run the fundamental and the second harmonic pulses are launched with zero group delay compensation $\tau_{\mathrm{gd}} = 0$ and arbitrary carrier phase offset φ. The actual delay τ_{gd} of the second harmonic pulse attained in the maximum plasma position was found and substituted into the second and the third runs with the initial conditions (7).

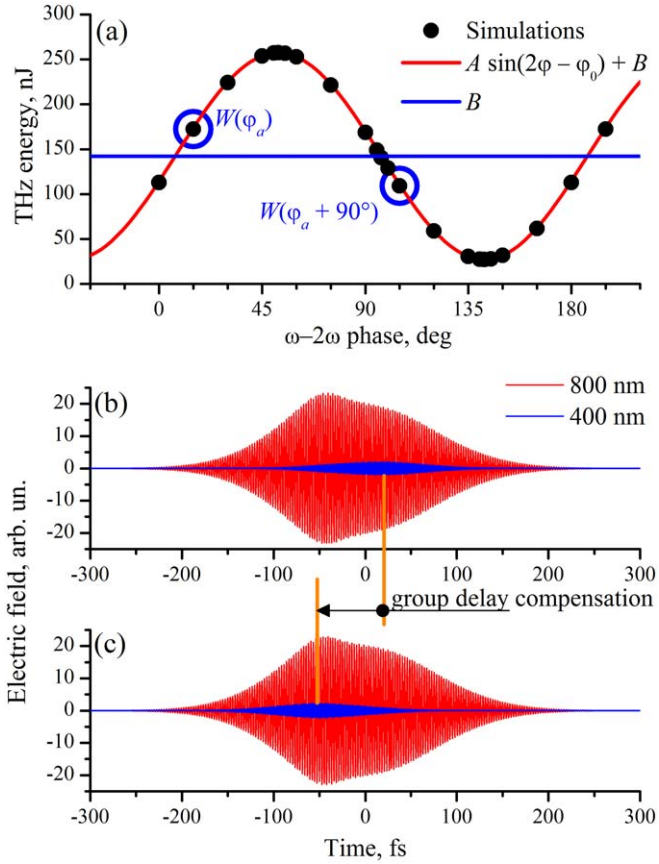

Figure 5. Obtaining the actual THz energy in the simulations: (a) black dots show the THz energy obtained as the result of the full propagation problem for the selected initial phase offsets between the first and the second harmonic pulses. Red solid curve shows the sinusoidal fit for the THz yield as the function of the initial phase offset φ. Blue horizontal line shows the average THz energy obtained by averaging of two THz energy values obtained for the initial phase offsets between the first and the second harmonic separated by 90° (e.g. the two dots inside the blue circles). (b), (c) The fundamental and the second harmonic pulse in the filament (b) without and (c) with group delay compensation.

These two runs are aimed at averaging the random fluctuations of the phase offset φ between ω and 2ω carrier waves. Indeed, the overall THz yield W_{THz} follows the sine dependence figure 5(a) as the function of the ω–2ω phase offset [9]

$$W_{\mathrm{THz}} = A\sin(2\varphi - \varphi_0) + B, \tag{8}$$

where we assume $B \geqslant A > 0$. Averaging of any two THz yields obtained from the phase offsets with the interval 90° (figure 5(a), circled dots) is equivalent to THz radiation energy averaging over all possible ω–2ω phase offsets. Exactly this averaged THz energy (equals to B in equation (8)) obtained in air or CO_2 is plotted as the function of pressure in figures 7, 8. Note that the phase φ_0 where $W_{\mathrm{THz}} = B$, as well as the 'optimized' group delay τ_{gd} depend on the pressure and are initially unknown, so it would be impossible to reconstruct the experimental curve using lesser amount of solver runs. If one just changes the pressure in the model, but preserves the group delay τ_{gd} and the phase φ to be zero in equation (7), the output THz yield will be affected by the three effects: pressure change itself, group walk-off that increases with pressure and random value of the ω–2ω carrier phase shift (figure 5(a)) leading to an order of magnitude yield uncertainty.

4. Terahertz energy in the experiment and simulations

In numerical simulations frequency-angular spectra were obtained for the air (figures 6(a)–(e)) and CO_2 (figures 6(f)–(j)) under different pressures.

Angular divergence increases with the pressure in both gases studied. In figure 6 vertical dashed line shows the collection angle 7.5° of the experimental setup. Already at 5 bar pressure in air (figure 6(d)) and 3 bar pressure in CO_2 (figure 6(h)) essential part of THz emission is transferred to the large angles and is not registered in the experiment. White curve in each panel indicates the fraction of THz energy propagating at given angle. We associate this increasing divergence with the plasma obstacle, which becomes stronger at higher pressures. Also it can be seen that in carbon dioxide angular divergence of THz emission is higher than in air. For the high pressure, for example 7 bar (figure 6(j)), almost all the THz emission obtained in CO_2 diverges at more than 10°.

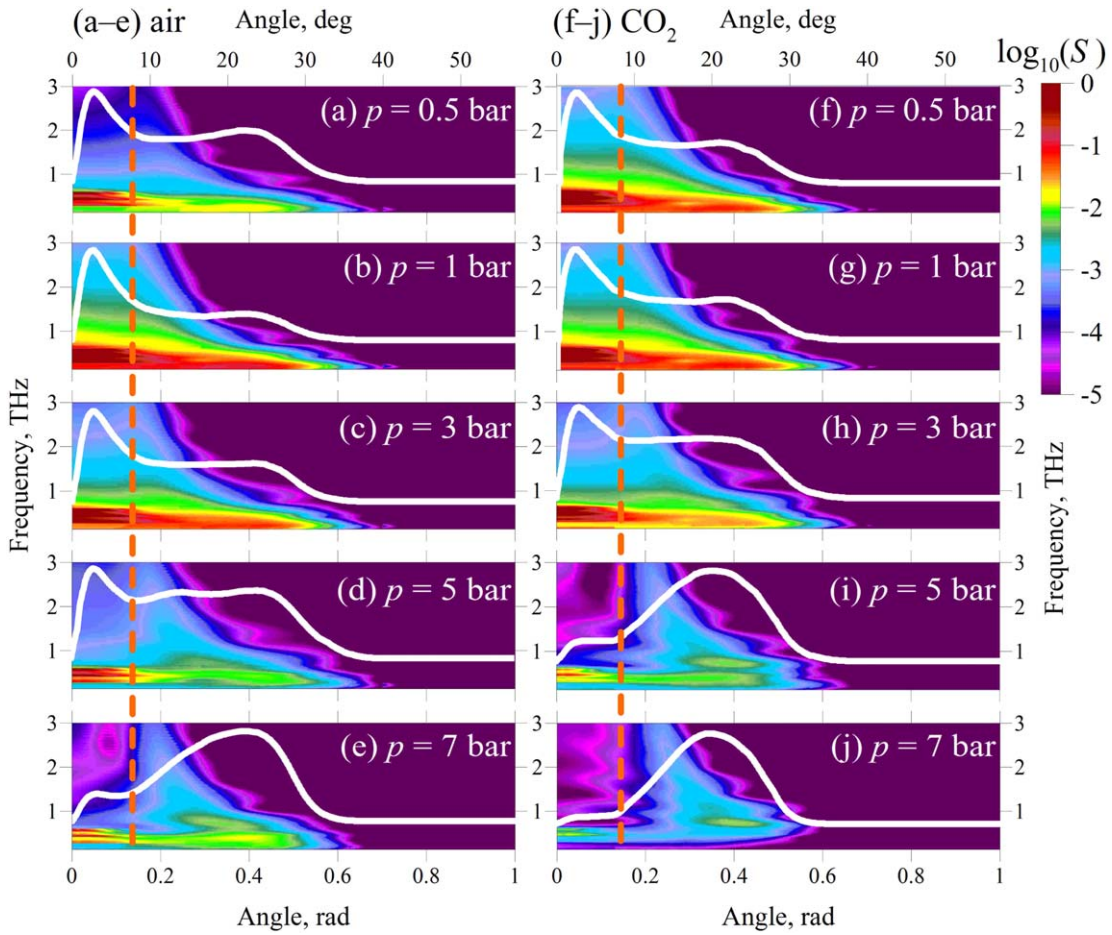

Figure 6. Angular-frequency spectra S of THz emission in air ((a)–(e), left column) and CO_2 ((f)–(j), right column) under different pressures. The spectral intensity S is normalized to the overall maximum value reached in air at 1 bar pressure, and the logarithmic color scale is the same for all panels (a)–(j). Vertical dashed lines indicate collection angle in the experiment. White curves show the angular distribution of THz energy $\mathrm{d}W/\mathrm{d}\theta = 2\pi\theta\int S(\theta, \omega)\,\mathrm{d}\omega$, where $\theta = \mathrm{asin}(ck_r/\omega)$.

Under the same 7 bar pressure of air the THz emission propagating along the beam axis is larger than in carbon dioxide (compare figure 6(e) and (j)). This difference in the angular divergence for two gases explains faster decrease of THz yield with pressure in CO_2 as compared with air, since both THz yields are collected in the same 15° angle (see figures 7(a), (b)).

To reproduce the THz yield in the experiment (see figure 4) we took into account the cuvette windows transmission cut-off at 1.5 THz (see figure 3) and detection setup overall collection angle of 7.5° from each side with respect to the beam axis (15° cone angle). The 'collected' in the simulations THz radiation is in agreement with the experimental THz yield in air (compare filled and empty circles in figure 7(a)). The maximum is achieved at 1 bar pressure, and the gradual decrease with the pressure is due to increasing divergence of THz radiation.

The simulated THz yield in carbon dioxide qualitatively reproduces the experimentally obtained data on the abrupt decay of THz energy with decreasing pressure below 1 bar and its slow decay with increasing pressure till 10 bars (compare filled circles and empty squares in figure 7(b)). The shift of the position of the maximum THz yield in the simulations from the one in the experiment might be associated with the contribution of the resonant nonlinear response of CO_2 molecule which was not considered in our model.

5. Optimal pressure for plasma generation and THz yield

The major mechanism of THz generation from two-color femtosecond breakdown is transient photocurrent in self-produced laser plasma [9, 10]. Therefore, the THz yield and the peak plasma density are expected to reveal the similar dependence on the gas pressure p. This expectation is fully confirmed by our simulations. The energy of electromagnetic radiation $W_{\mathrm{THz}}(p)$ from the two-color filament is integrated over half-a-sphere, i.e. in the angle of 90° from each side to the beam axis, and up to 20 THz in the frequency domain for all pressures p

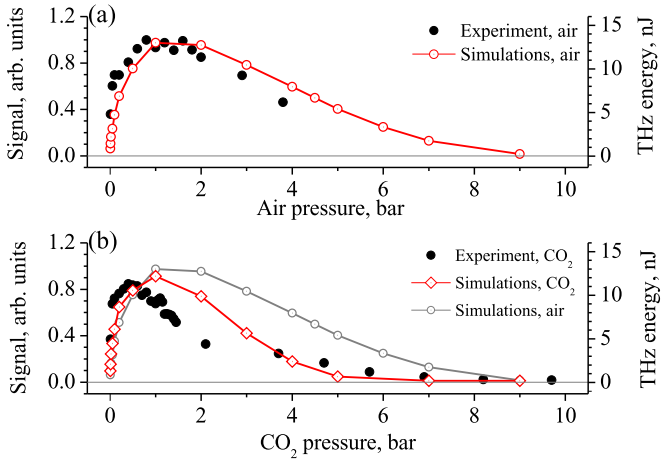

Figure 7. The comparison of THz energy in the experiment (left axis) and simulations (right axis) for (a) air and (b) carbon dioxide. Gray dots in (b) are a replica of red ones in (a). In simulations, the THz field only up to frequency of 1.5 THz and divergence angle of 7.5° was collected according to experimental detection scheme.

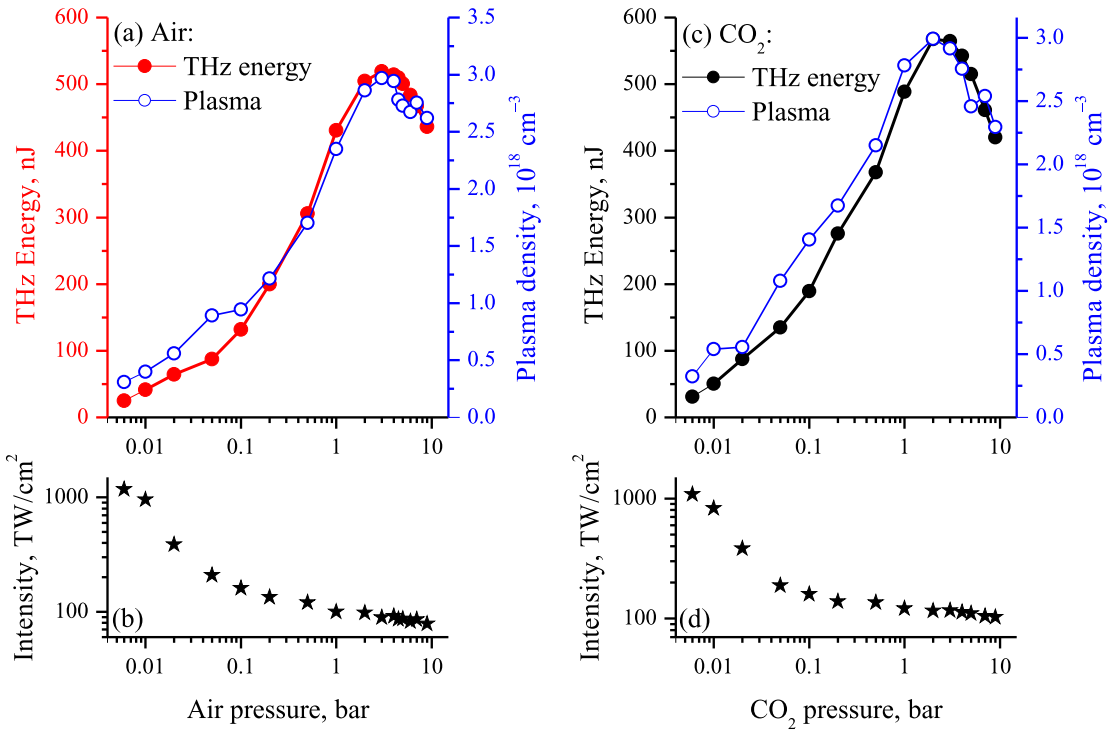

Figure 8. (a), (c) The comparison of THz energy obtained in numerical simulations integrated in a hemisphere and the frequency range 0.07–20 THz for air (red dots, left axis, panel a) and carbon dioxide (black dots, left axis, panel c) with the peak plasma density (blue open circles, right axis). (b), (d) Peak optical pulse intensity dependence on pressure for air (b) and CO_2 (d).

studied. This energy $W_{\mathrm{THz}}(p)$ follows closely the peak plasma density $N_{\mathrm{peak}}(p)$ for both air and CO_2 (figure 8, upper row, panels (a) and (c), compare filled and empty circles in each panel).

In particular, the maxima of the dependencies $W_{\mathrm{THz}}(p)$ and $N_{\mathrm{peak}}(p)$ match perfectly (3 bar for air and 2 bar for CO_2). Thus, the search for the pressure giving the optimum THz yield corresponds to the search for the maximum plasma density. Plasma density is, in turn, defined by the peak intensity I_{peak} in the filament (figure 8, lower row).

The monotonic decrease of the peak intensity $I_{\mathrm{peak}}(p)$ with the pressure p growth can be explained from the similarity approach as follows. The propagation of the optical harmonics in the focusing conditions of our experiment (numerical aperture NA $\approx a_0/F \approx 10^{-2}$), where F is the geometrical focusing distance, is paraxial, i.e. the longitudinal projection of the wave vector in equation (1) is $k_z \approx k - k_r^2/2k$. The paraxial approximation of UPPE with the current (6) preserves its formulation if the variables $\{x, y, z\}$ are replaced by

$\{x\sqrt{p}, y\sqrt{p}, zp\}$. Hence, the similarity parameters are $a_0\sqrt{p}$ and Fp, and the effective numerical aperture depends on the pressure as NA $\propto 1/\sqrt{p}$. Thus, the geometrical focusing becomes weaker with increasing pressure, while the 3rd-order nonlinearity in equation (3) and, hence, the self-focusing dominates the propagation.

The peak intensity in the filamentation regime (that is loose focusing or the collimated beam, where propagation is dominated by self-focusing) is defined by the clamped intensity $I_c \approx 70$ TW cm^{-2} [34, 35]. In contrast, the intensity of the femtosecond pulse focused in low pressure gases is about 1 PW cm^{-2}, just two times lower than the vacuum intensity for our focusing conditions $I_v \approx 2$ PW cm^{-2} calculated according to the linear diffraction theory. Correspondingly, radius of the first harmonic decreases from root-mean-square of 170 μm for 9 bar (this value is large due to strong diffraction on plasma obstacle) to 20 μm for 5 mbar (compare with the vacuum radius of 13 μm). The second harmonic is less sensitive to the pressure, so its radius decreases from 35 μm to 7.5 μm (the vacuum radius of 6.5 μm).

At the fixed peak intensity value the density of free electrons is proportional to the gas pressure. The growth of pressure accompanied by the decrease in the peak intensity (see lower row, filled circles on figure 8) provides us with the optimum (i.e. the largest) value of the peak plasma density and THz yield attained at 3 bars in air or 2 bars in CO_2 (figure 8 (upper row)).

6. THz emission from two-color optical breakdown in the atmosphere of Mars

The atmosphere of Mars is primarily composed of CO_2 (95%) under the pressure of 6 mbar [18]. Water vapor is a trace gas in the Martian atmosphere (~0.03% [20]). In the atmosphere of Mars THz radiation absorption length due to H_2O bands is ~3 orders of magnitude larger than in the atmosphere of Earth. The Martian dust particles cause essential attenuation of visible and infrared radiation (wavelength of ~1 μm) since the typical dust particle size is 0.6–2 μm [36]. Such dry scattering medium is expected to be transparent for THz radiation with the wavelength of ~100 μm. So, the THz radiation seems to be a prominent candidate for lidar and free-space communication applications in the atmosphere of Mars.

The lowest carbon dioxide pressure $p = 10$ mbar achieved in the cuvette used in our experiment reproduces the conditions of the Martian atmosphere adequately. The THz yield from two-color optical breakdown for $p = 10$ mbar is a factor of 2 lower than the optimal one in carbon dioxide at $p = 0.5$ bar (figure 7(b)) and a factor of 2.5 lower than the best yield from atmospheric air (figure 7(a)). In the simulations we can decrease the CO_2 pressure down to $p = 6$ mbar and remove the propagation in air from the laser system output to the cuvette.

Possible experimental setup for THz generation in the atmosphere of Mars can be realized using the collinear propagation of the first and the second harmonic of Ti:Sapphire laser. The doubling-frequency crystal might be inserted into the fundamental beam directly since the group walk-off between the optical harmonics will be minimized at low pressure and due to the absence of the cuvette window.

The phase delay φ between ω and 2ω fields allows us to maximize the THz yield as compared with the average one that is registered in the experiment with independently controlled ω and 2ω beams. Therefore, in numerical simulations we do not need the optimization of the group walk-off and can assume $\tau_{gd} = 0$ in the initial conditions (7). According to the sine dependence of THz energy W_{THz} on phase delay φ (see figure 5(a) and equation (8)) the maximum THz energy can be deduced from free runs with three different delays: $\varphi = \varphi_a$, $\varphi_a + 60°$ and $\varphi_a + 120°$, φ_a is an arbitrary phase delay between ω and 2ω fields. So, the maximum of THz energy is given by $W_{THz}^{(max)} = A + B$, where

$$A = \frac{\sqrt{2}}{3}\sqrt{\sum_{j,l=0}^{2}(3\delta_l^j - 1)\, W_{THz}^{(j)} W_{THz}^{(l)}}, \tag{9}$$

$$B = \frac{1}{3}\sum_{j=0}^{2} W_{THz}^{(j)}, \tag{10}$$

and $W_{THz}^{(j)} = W_{THz}(\varphi_a + j \times 60°)$, δ_j^l is the Kronecker delta.

The optical breakdown in the Martian atmosphere is characterized by full double ionization of carbon dioxide. This double ionization with the second ionization potential of carbon dioxide equal to 22.4 eV is possible because of the high 1 PW cm^{-2} intensity reached in the geometric focus in a low-pressure (6 mbar) gas. This overall maximum in the medium is just a factor of 2 lower than the vacuum intensity in the geometrical focus (figure 9(a)). Arrest of the intensity growth occurs due to the plasma-induced defocusing in the plasma with the electron density of $N_{peak} = 3.24 \times 10^{17}$ cm^{-3} (figure 9(b)) at the intensity of 1 PW cm^{-2}. For comparison, the maximum intensity in the atmosphere of Earth is one order of magnitude lower, while the maximum plasma density is one order of magnitude higher (figure 10).

The total THz yield available near the surface of Mars is 76 nJ (figures 9(b) and 10), i.e. six times lower than in the atmosphere of Earth (430 nJ), see figure 10 (the left vertical bars). Within the cone with 15° at the vertex and

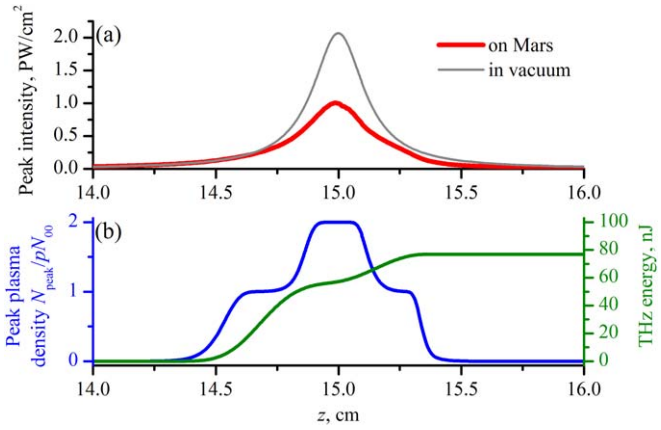

Figure 9. THz generation from 125 fs 1.4 mJ 800 + 400 nm pulse focused by 15 cm lens near the surface of Mars (the pressure of CO_2 is 6 mbar). (a) Peak intensity at each position along the propagation direction (red curve) and the one in vacuum (grey curve). (b) Peak plasma density (blue curve, left axis) and THz energy (green curve, right axis) at each position along the propagation direction. Here $N_{00} = 2.7 \times 10^{19}$ cm^{-3} is the gas density at atmospheric pressure.

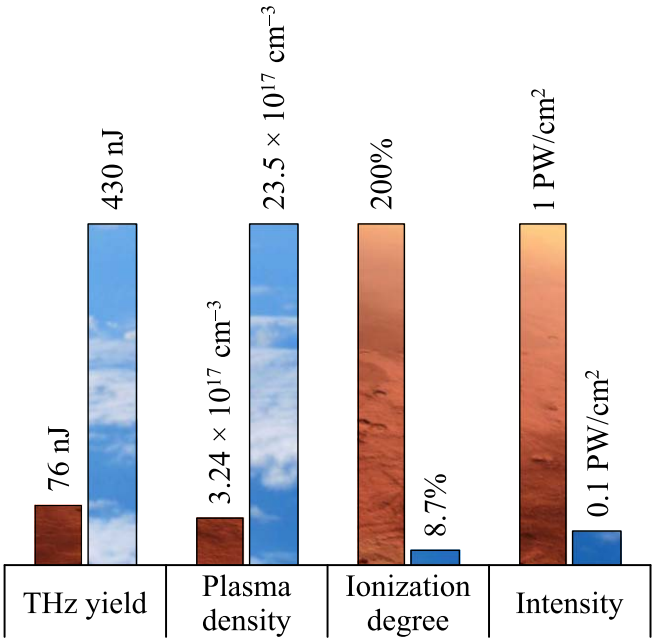

Figure 10. The comparison of THz yield and femtosecond optical breakdown parameters in the atmosphere of Mars and Earth.

frequency integrated from 0 to 1.5 THz the energy of THz radiation is 0.6 nJ. Thus, the extremely high intensity during the focusing of a femtosecond pulse in the 6 mbar Martian atmosphere provides the efficient THz emission, which is slightly weaker than on the Earth's surface.

7. Conclusions

In our work we have shown experimentally the possibility of using carbon dioxide to generate broadband THz radiation in a 'two-color' laser field, and found the optimal pressure for the generation of THz pulses. The obtained results demonstrate that the main source of THz radiation generation are free electrons, the absolute number of which in the focal region is determined by both the gas pressure and the pump pulse intensity. The pressure increase results in the decrease in the pulse intensity from ~1 PW cm^{-2} to ~100 TW cm^{-2} due to continuous transmission from focusing into vacuum to filamentation with the clamped intensity. As a result, the ionization rate decreases simultaneously with the gas density growth thus providing the maximum in the plasma

density and the THz yield. The THz energy at low pressures ~0.01 bar is only a few times lower than the maximum value due to the full double ionization under the extremely high intensity.

The results of our research on the generation of THz radiation of CO_2 can be used to estimate the potential applicability of femtosecond laser-induced THz generation as a method to study the planetary atmospheres of Mars and Venus. So, we can make a conclusion that the generation of THz radiation in low-pressure atmosphere of Mars can be effective. Moreover, due to low absorption and dispersion of THz radiation in this atmosphere, its further propagation for long distances is also possible. All these taken together allow us to consider laser-induced THz generation as a promising tool for remote sensing of the Martian atmosphere.

Acknowledgments

This work was partially supported by the Russian Foundation for Basic Research under Grants 18-52-16016, 18-29-20104, 17-02-01217, 18-52-16020, 18-32-01000, 18-02-00954. This work was supported in part by the National Natural Science Foundation of China (61722111), the 111 Project (D18014), the International Joint Lab Program supported by Science and Technology Commission Shanghai Municipality (17590750300). This work was partially supported by the Ministry of Science and Higher Education within the State assignment FSRC 'Crystallography and Photonics' RAS and NUST MISIS Competitiveness Program by the Ministry of Science and Higher Education of Russian Federation (No. K2-2019-004). DES thanks the Scholarship of the Russian Federation President (SP-2 453.201 8.2) and Foundation for the Advancement of Theoretical Physics and Mathematics 'BASIS'.

ORCID iDs

Nikita V Minaev https://orcid.org/0000-0002-9931-0118
Olga G Kosareva https://orcid.org/0000-0002-5754-1057

References

[1] Askaryan G 1962 *Sov. Phys. JETP* **15** 943
[2] Cherenkov P 1938 *Sci. URSS* **21** 319–21
[3] Hamster H, Sullivan A, Gordon S, White W and Falcone R 1993 *Phys. Rev. Lett.* **71** 2725
[4] Cook D and Hochstrasser R 2000 *Opt. Lett.* **25** 1210–2
[5] Zhang X C and Xu J 2010 *Introduction to THz Wave Photonics* vol 29 (Berlin: Springer)
[6] Jin Q, Dai J E Y and Zhang X C 2018 *Appl. Phys. Lett.* **113** 261101
[7] Balakin A V, Garnov S V, Makarov V A, Kuzechkin N A, Obraztsov P A, Solyankin P M, Shkurinov A P and Zhu Y 2018 *Opt. Lett.* **43** 4406–9
[8] Zhang X C, Shkurinov A and Zhang Y 2017 *Nat. Photon.* **11** 16
[9] Kim K Y, Glownia J H, Taylor A J and Rodriguez G 2007 *Opt. Express* **15** 4577–84
[10] Andreeva V *et al* 2016 *Phys. Rev. Lett.* **116** 063902
[11] Andreev A V and Stremoukhov S Y 2013 *Phys. Rev.* A **87** 053416
[12] Löffler T and Roskos H 2002 *J. Appl. Phys.* **91** 2611–4
[13] Thomson M D, Kreß M, Löffler T and Roskos H G 2007 *Laser Photonics Rev.* **1** 349–68
[14] Rodriguez G and Dakovski G L 2010 *Opt. Express* **18** 15130–43
[15] Manceau J M, Massaouti M and Tzortzakis S 2010 *Opt. Express* **18** 18894–9
[16] Yoo Y J, Jang D and Kim K Y 2019 *Opt. Express* **27** 22663–73
[17] Mittleman D 2013 *Sensing with Terahertz Radiation* vol 85 (Berlin: Springer)
[18] Franz H B *et al* 2017 *Planet. Space Sci.* **138** 44–54
[19] Basilevsky A T and Head J W 2003 *Rep. Prog. Phys.* **66** 1699
[20] Trokhimovskiy A, Fedorova A, Korablev O, Montmessin F, Bertaux J L, Rodin A and Smith M D 2015 *Icarus* **251** 50–64
[21] Kolesik M and Moloney J V 2004 *Phys. Rev.* E **70** 036604
[22] Mareev E, Aleshkevich V, Potemkin F, Bagratashvili V, Minaev N and Gordienko V 2018 *Opt. Express* **26** 13229–38
[23] Kosareva O *et al* 2018 *Opt. Lett.* **43** 90–3
[24] Bergé L, Skupin S, Köhler C, Babushkin I and Herrmann J 2013 *Phys. Rev. Lett.* **110** 073901
[25] Fedorov V Y and Tzortzakis S 2018 *Phys. Rev.* A **97** 063842
[26] Wood W M, Siders C W and Downer M 1993 *IEEE Trans. Plasma Sci.* **21** 20–33
[27] Hosseini S, Kosareva O, Panov N, Kandidov V, Azarm A, Daigle J, Savel'ev A, Wang T and Chin S 2012 *Laser Phys. Lett.* **9** 868
[28] Lide D R 2004 *CRC Handbook of Chemistry and Physics* vol 85 (Boca Raton, FL: CRC Press)
[29] Rothman L *et al* 2013 *J. Quant. Spectrosc. Radiat. Transfer* **130** 4–50
[30] Bideau-Mehu A, Guern Y, Abjean R and Johannin-Gilles A 1973 *Opt. Commun.* **9** 432–4
[31] Borodin A V, Panov N A, Kosareva O G, Andreeva V A, Esaulkov M N, Makarov V A, Shkurinov A P, Chin S L and Zhang X C 2013 *Opt. Lett.* **38** 1906
[32] Schuh K, Rosenow P, Kolesik M, Wright E M, Koch S W and Moloney J V 2017 *Phys. Rev.* A **96** 6–11
[33] Zhang Z *et al* 2018 *Appl. Phys. Lett.* **113** 241103
[34] Kasparian J, Sauerbrey R and Chin S L 2000 *Appl. Phys.* B **71** 877
[35] Kosareva O G *et al* 2009 *Laser Phys.* **19** 1776–92
[36] Montabone L *et al* 2015 *Icarus* **251** 65–95